JOURNAL OF MECHANICS OF CONTINUA AND MATHEMATICAL SCIENCES
www.journalimcms.org

ISSN (Online) : 2454 -7190 Vol.-21, No.-04, April (2026) pp 1-17 ISSN (Print) 0973-8975

DESIGN AND OPTIMIZATION OF A TRIBAND STAR-SHAPED MIMO MICROSTRIP PATCH ANTENNA FOR KU-BAND APPLICATIONS

Touko Tcheutou Stephane Borel[1], Rashmi Priyadarshini[2]

[1,2]Department of Electronics and Communication Engineering, Sharda University, Greater Noida, India.

Email: [1]stephtouko@yahoo.com, [2]rashmi.priyadarshini@sharda.ac.in

Corresponding author: **Touko Tcheutou Stephane Borel**

https://doi.org/10.26782/jmcms.2026.04.00001

(Received: January 29, 2026; Revised: April 02, 2026; Accepted : April 12, 2026)

Abstract

This paper presents the design, optimization, and experimental validation of a triband star-shaped microstrip patch antenna for Ku-band applications. The design process begins with a single star-shaped patch antenna, which is progressively improved and extended to form a multiple-input multiple-output (MIMO) configuration. The final optimized MIMO antenna operates within 12–16 GHz, achieving resonances at 12.3 GHz, 14.2 GHz, and 15 GHz. The star-shaped geometry is employed to enhance the impedance bandwidth and improve gain performance. Simulated and measured results show good agreement in terms of return loss, impedance bandwidth, voltage standing wave ratio (VSWR), and radiation patterns. Moreover, diversity performance metrics, including the envelope correlation coefficient (ECC) and diversity gain (DG), confirm low correlation and near-ideal diversity across the three operating bands. The proposed triband MIMO antenna exhibits stable radiation performance and satisfactory gain, making it a strong candidate for 5G and satellite communication systems in the Ku-band.

Keywords: MIMO, Patch Antenna, Ku-Bands, Star shape

I. Introduction

The rapid growth of wireless communication systems, satellite networks, and emerging 5G/6G technologies has stimulated significant research interest in the development of compact and high-performance antennas. In particular, the Ku-band (12–18 GHz) plays a vital role in satellite broadcasting, radar sensing, and high-capacity terrestrial links, making it an attractive spectrum for next-generation communication systems [I, III]. To meet the requirements of such applications, antennas must exhibit wide impedance bandwidth, stable radiation patterns, and satisfactory gain, while maintaining a compact size suitable for integration into modern devices. Microstrip patch antennas have become one of the most promising solutions due to their low profile, lightweight structure, ease of fabrication, and compatibility with planar circuits. However, conventional rectangular and circular patch antennas

suffer from narrow bandwidth and limited gain, which restricts their applicability in high-frequency and broadband communication systems. To overcome these limitations, numerous techniques have been proposed, including the introduction of slots, defected ground structures (DGS), parasitic elements, and modifications of the radiating geometry [VI, IX]. In recent years, triband and multiband patch antennas have gained particular attention for their ability to support multiple services with a single structure. For example, [I] reported a compact dual-band patch antenna for satellite communication, while [II] proposed a wideband slot-loaded antenna for 5G applications. Similarly, [III] demonstrated a high-gain triband MIMO antenna designed for X- and Ku-band satellite links. Despite these advancements, achieving a compact triband design with optimized gain and robust MIMO performance remains a significant challenge. Multiple-input multiple-output (MIMO) technology is a key enabler for modern wireless systems, as it enhances spectral efficiency, reliability, and channel capacity by exploiting multipath propagation. For efficient MIMO operation, antennas must demonstrate high isolation, low envelope correlation coefficient (ECC), and near-ideal diversity gain (DG) [XV, XVI, XX].

The integration of multiband operation with MIMO performance is therefore essential to meet the stringent requirements of 5G and satellite systems in the Ku-band [XXII, XXIX]. Motivated by these challenges, this paper presents the design, optimization, and experimental validation of a triband star-shaped microstrip patch antenna, progressively evolved from a simple single-element design to a final optimized MIMO configuration. The initial star-shaped geometry improves impedance matching and enhances bandwidth, while successive design iterations lead to the realization of a compact triband MIMO antenna resonating at 12.3 GHz, 14.2 GHz, and 15 GHz. Both simulated and measured results are analyzed in terms of return loss, voltage standing wave ratio (VSWR), gain, and radiation patterns. In addition, diversity parameters such as ECC and DG are evaluated to demonstrate the suitability of the proposed antenna for MIMO operation. The fabricated prototype confirms the validity of the design, showing good agreement with simulations.

II. Antenna Design and Methodology

a. Substrate and General Specifications

The antenna is fabricated on an FR-4 substrate having a relative permittivity of 4.4, a thickness of 1.6 mm, and an overall size of 41.5 × 30 mm^2. The copper cladding thickness of the patch and ground plane is 35 μm. While FR-4 is a popular substrate due to its low cost, ease of fabrication, and availability, it is well known that FR-4 has relatively high dielectric losses at Ku-band frequencies. To account for this effect, the dielectric loss tangent (tanδ) of the substrate has been included in the simulation, with a value of 0.02, which is typical in the 10-15 GHz range. Furthermore, the loss tangent of FR-4 increases with frequency, and as such, the dielectric losses are even higher at higher operating frequencies.

However, FR-4 remains an attractive substrate for practical, cost-sensitive applications, especially for large-scale production. In this paper, FR-4 has a good compromise between performance and fabrication cost while still achieving satisfactory radiation characteristics at Ku-band.

To further emphasize the effect of the losses of the substrate, a comparison with a low-loss substrate (Rogers RT/Duroid 5880, εr = 2.2, tanδ = 0.0009) is included in the Results section.

b. Stepwise Design Evolution

The antenna development followed a systematic three-step evolution, where each step introduced specific modifications to enhance resonance characteristics, improve gain, and enable MIMO operation.

The first design, Antenna 1, consists of a single star-shaped microstrip patch fed by a 50-Ω microstrip line. The star geometry was deliberately selected because it alters the surface current paths, creating multiple effective resonances and thereby enhancing the potential for triband operation within the Ku-band. This antenna provided initial resonant modes but exhibited limited gain and no diversity since it was a single-element configuration. Figure 1 shows the geometry of Antenna 1.

In the second design, Antenna 2, a second identical star-shaped patch was introduced to form a MIMO configuration. In this case, the two ports were placed on **opposite sides of the substrate**, creating a mirrored configuration. This layout improved isolation between the two elements because of the spatial separation, while maintaining compact overall dimensions. The resulting antenna exhibited improved impedance bandwidth and enhanced resonant behavior compared to Antenna 1, along with the added advantage of MIMO diversity. However, the opposite-feed layout created some asymmetry in radiation, which required further refinement. Figure 1 depicts the layout of Antenna 2 with ports located on opposite sides.

The third and final design, Antenna 3, represents the optimized triband MIMO antenna. In this version, two star-shaped patches were retained, but the feed ports were placed on the **same side of the substrate**. This arrangement not only facilitated a more compact and practical feed network design but also ensured symmetrical radiation performance and improved integration possibilities. Careful optimization of the patch geometry, inter-element spacing, and feed positioning resulted in clear and stable resonances at 12.3 GHz, 14.2 GHz, and 15.0 GHz. The final antenna also demonstrated enhanced realized gain and excellent MIMO performance, validated later through envelope correlation coefficient (ECC) and diversity gain (DG) analysis. Figure 1 illustrates the geometry of this optimized design with both ports on the same side.

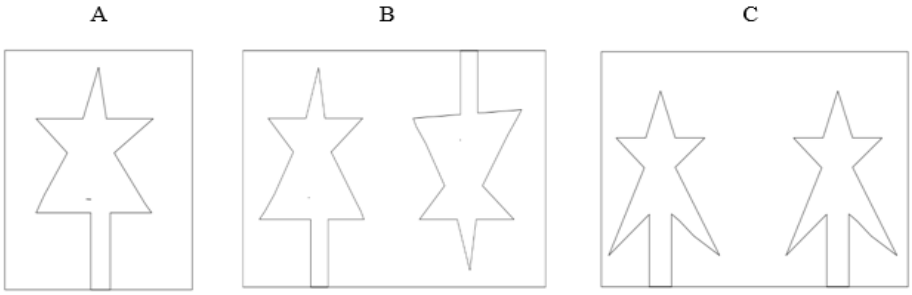

Fig. 1. Evolution of the design. (A) Antenna 1, (B) Antenna 2, and (C) Antenna 3, or the proposed antenna

Table 1: Dimensions of the Proposed Antenna

Parameters	Dimensions (mm)	Parameters	Dimensions (mm)
Ls	41.5	F	3
Ws	30	G	4
A	6.33	H	8.38
B	12.75	I	4
C	5.4	J	5.48
D	24	K	12.17
E	9.26	L	7.61

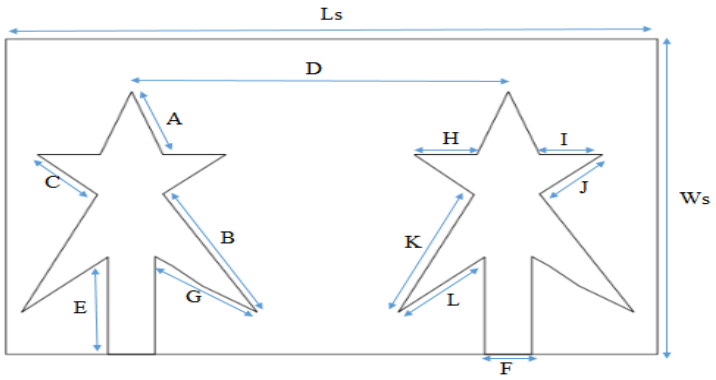

Fig. 2. Proposed star MIMO antenna

III. Results and Discussion

a. Reflection Coefficient And Bandwidth Analysis

The reflection coefficient (S11) of the three proposed antenna designs was analyzed to evaluate the matching performance and the evolution of resonant frequencies. Figure 3 presents the comparative S11 plots of Antenna 1, Antenna 2, and Antenna 3.

For Antenna 1, the single star-shaped patch generated initial resonances within the Ku-band, but the return loss levels were not sufficiently deep, indicating poor impedance

matching. The reflection coefficient was only slightly below –10 dB across a narrow bandwidth, which limited its practical performance.

In Antenna 2, where two star-shaped patches were introduced with ports located on opposite sides of the substrate, the S11 response improved significantly. Multiple resonances appeared with deeper return loss values, confirming better impedance matching. The isolation provided by the opposite feed configuration also contributed to a more stable return loss curve. However, while the triband response began to emerge, some resonances remained shallow and required further optimization.

The final configuration, Antenna 3, exhibited the best performance. The return loss plot shows three well-defined resonances: the first centered at 12.3 GHz with a bandwidth from 12.09 to 12.70 GHz and a return loss of –19.62 dB, the second centered at 14.2 GHz with a bandwidth from 13.67 to 14.67 GHz and a return loss of –18.98 dB, and the third centered at 15.0 GHz with a bandwidth from 14.67 to 16 GHz and a return loss of –17.10 dB. These results confirm excellent impedance matching across the three operational bands. Compared to Antenna 1 and Antenna 2, the resonant frequencies of Antenna 3 were more stable and covered wider bandwidths. The achieved triband operation demonstrates the effectiveness of the optimized star-shaped geometry and the placement of both ports on the same side of the substrate.

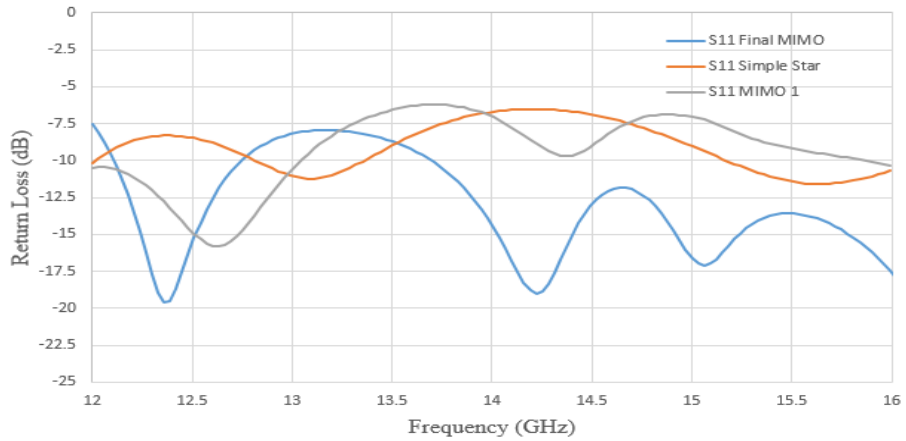

Fig. 3. Comparison between S11 of the different antennas

These results confirm that the design progression from Antenna 1 to Antenna 3 significantly improved impedance bandwidth and matching quality, leading to a high-performance triband MIMO antenna suitable for Ku-band applications.

To check the impact of the substrate material on the impedance matching, a comparative investigation of the reflection coefficient (S11) was carried out through FR-4 and Rogers RT/Duroid 5880 substrates. It is observed that the FR-4-based antenna provides a clean triband response with distinct resonances at 12.3 GHz, 14.2 GHz, and 15 GHz, whereas the Rogers-based antenna shows a significant shift in the resonance behavior, where it has only one dominant resonance at 12.3 GHz, and the other resonances do not fulfill the matching condition (S11 < -10 dB).

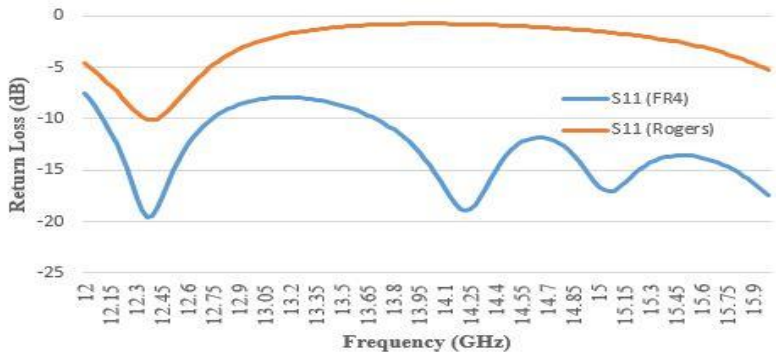

Fig. 4 Comparison of the reflection coefficient (S11) of the proposed antenna using FR-4 and Rogers RT/Duroid 5880 substrates.

This difference is mainly due to the change in the dielectric constant between the two substrates, which has a significant impact on the effective electrical length of the antenna and shifts the resonant frequencies.

These findings show that the proposed antenna geometry is optimized only for the FR-4 substrate, and a re-optimization would be needed to achieve the desired multiband response of the antenna using another substrate.

b. Gain (G), Directivity (D), and Efficiency (η)

The radiation performance of the three designs was evaluated in terms of simulated realized gain (G) and directivity (D). The progression from Antenna 1 to Antenna 3 reveals a consistent improvement in both metrics, reflecting the benefits of geometry refinement and feed configuration.

For Antenna 1, the simulated values are G = 1.23 dB and D = 3.67 dB across its operating resonances. These results indicate limited radiation efficiency and relatively weak directivity, which is consistent with the single-element configuration and its non-optimized matching.

For Antenna 2, which introduces a MIMO arrangement with ports on opposite sides, the simulated values increase to G = 3.94 dB and D = 5.82 dB. The improvement in both G and D confirms that the dual-element arrangement and the accompanying impedance refinement strengthen the main lobe while containing unwanted radiation. Some asymmetry persists due to the opposite-side feeds, which motivates further optimization.

For Antenna 3, the final optimized MIMO design with both ports on the same side yields simulated results of G = 6.18 dB and D = 7.87 dB. This configuration achieves the highest gain and directivity among the three designs, yielding a more concentrated main beam and more stable patterns across the three operating bands.

An additional indicator of improvement is the simulated radiation efficiency, which can be inferred from the G–D gap. Using the equation below [XVII]:

$$\eta = 10^{\frac{G-D}{10}} \quad (1)$$

The efficiency evolves from roughly 57% for Antenna 1 (1.23 dB vs. 3.67 dB) to about 65% for Antenna 2 (3.94 dB vs. 5.82 dB) and up to approximately 68% for Antenna 3 (6.18 dB vs. 7.87 dB). According to Ku-band antenna standards, a minimum radiation efficiency of 60% is generally required for practical applications such as satellite links and high-frequency 5G applications. It can therefore be concluded that while Antenna 1 falls below this requirement, both Antenna 2 and Antenna 3 satisfy and exceed the minimum efficiency threshold, with the final design offering the most robust margin. Overall, the radiation analysis demonstrates that the stepwise evolution from a single star-shaped patch to the final MIMO configuration produces marked gains in both realized gain and directivity, with the Antenna 3 design offering the most favorable balance for Ku-band triband operation.

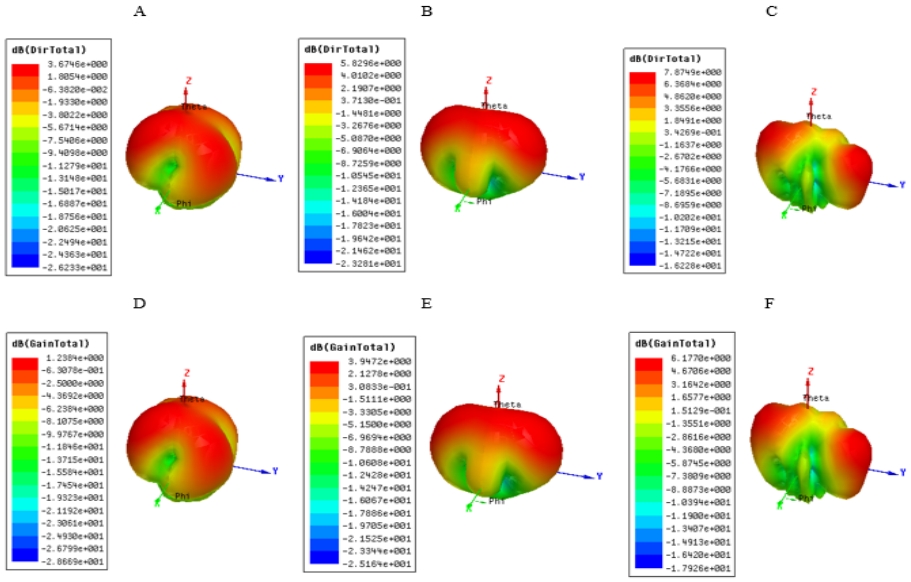

Fig. 5. Simulated radiation patterns and comparison of Directivity and Gain for Antenna 1 (A and D), Antenna 2 (B and E), and Antenna 3 (C and F).

Figures 6 and 7 show the comparison between the realized gain and radiation efficiency of the proposed antenna when FR-4 and Rogers RT/Duroid 5880 substrates are used. As can be seen, the antenna using Rogers has a better realized gain (approximately 7.3 dB at 12.3 GHz), since its dielectric losses are much smaller. On the other hand, the proposed antenna using FR-4 substrate has a lower gain (up to 6.18 dB). Likewise, the antenna with the Rogers substrate also has a better radiation efficiency, due to its small loss tangent. Nevertheless, as we can see, the antenna does not preserve its triband behavior with Rogers, since only one resonance satisfies the matching condition (S11 < -10 dB), while the other bands are displaced.

This behavior is mainly because the dielectric constant is different, which changes the effective electrical dimensions of the antenna and the resonance frequencies. Although the gain and efficiency are lower, the multiband operation of the antenna using FR-4

substrate is stable, and therefore it is better suited for practical applications in the Ku-band. These results show that the proposed antenna provides a good compromise between performance and cost.

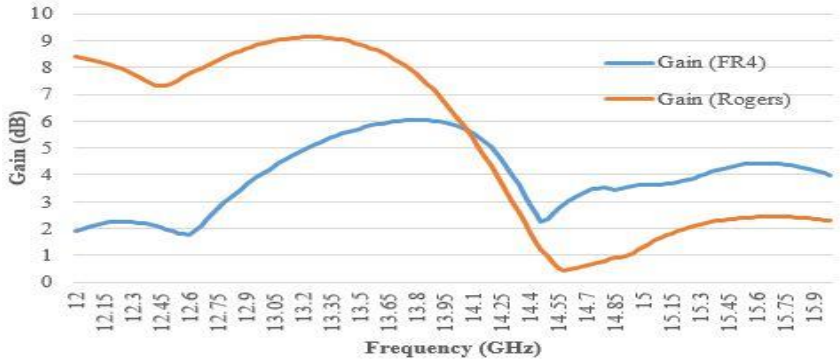

Fig. 6. Comparison of the realized gain versus frequency for the proposed antenna using FR-4 and Rogers RT/Duroid 5880 substrates.

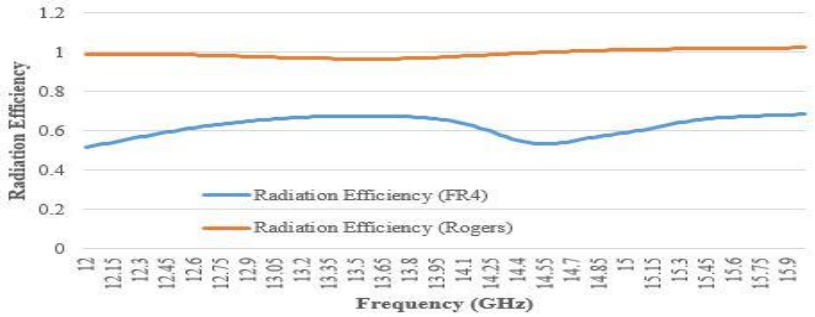

Fig. 7. Comparison of the radiation efficiency versus frequency for the proposed antenna using FR-4 and Rogers RT/Duroid 5880 substrates.

c. Mutual Coupling and Isolation (S21)

An essential parameter for evaluating the performance of a MIMO antenna is the mutual coupling between the radiating elements, expressed in terms of the transmission coefficient S21 [X, XXIII]. High isolation ensures low correlation between the antenna ports and supports the diversity performance required for advanced wireless systems. For the final Antenna 3 design, the simulated S21 remains consistently below −20 dB across all three operating bands (12.3 GHz, 14.2 GHz, and 15 GHz).

This level of isolation is significantly better than the commonly accepted threshold of −15 dB for practical MIMO systems, thereby confirming excellent port decoupling. The achieved isolation not only reduces mutual interference but also improves other MIMO performance indicators, such as the envelope correlation coefficient (ECC) and diversity gain (DG), which will be discussed in the following section. Thus, the optimized geometry of Antenna 3 ensures reliable operation in Ku-band triband scenarios.

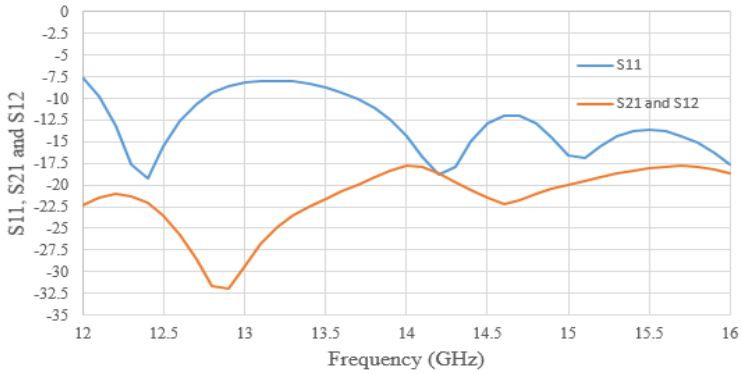

Fig. 8. Simulated S21 of the proposed Antenna

d. Envelope Correlation Coefficient (ECC) and Diversity Gain (DG)

The envelope correlation coefficient (ECC) is a key parameter for the characterization of the diversity performance of MIMO antennas. In this paper, the ECC is estimated using S-parameters, which is a simplified and common approximation. This approximation assumes a lossless environment with a uniform propagation velocity and does not consider the characteristics of the radiation patterns. An accurate evaluation can be achieved using far-field radiation patterns. Nevertheless, due to the very low mutual coupling between antenna elements (S21 < -20 dB), the S-parameter-based approximation is still valid in this case.

The ECC values obtained are below 0.004 throughout the operating bands, showing a good diversity performance and a low correlation between the signals received by the antenna elements. Ideally, ECC should be close to zero, with values below 0.5 considered acceptable for practical systems [XVIII, XIX, XXV]. One common formulation exists: Based on S-parameters (commonly used for lossless 2 x 2 MIMO antennas):

$$\rho_{12} = \frac{|S_{11}*S_{12}+S_{21}*S_{22}|}{(1-|S_{11}|^2-S_{12}{}^2)(1-|S_{21}|^2-S_{22}{}^2)} \quad (2)$$

As illustrated in Figure 7, ECC, the proposed antenna achieves an ECC of less than 0.004 across the operating band, which demonstrates extremely low correlation between antenna elements. This is consistent with the measured isolation of S21 < –20 dB.

The Diversity Gain quantifies the improvement in reliability due to multiple uncorrelated radiation patterns. In Multiple Input Multiple Output (MIMO) systems, diversity gain (DG) is a performance indicator that measures the improvement in the system's ability to combat signal dropouts and interference compared to a single-antenna system [XII, XIII]. It basically means the power reduction required to maintain the same signal reliability. A high DG ratio indicates a more robust system, ensuring more stable communication despite signal variations. It is usually determined by the envelope correlation coefficient (ECC), with a high DG meaning a low ECC.

For a 2 x 2 MIMO system, it is given by:

$$DG = 10\sqrt{1-|ECC|^2} \quad (3)$$

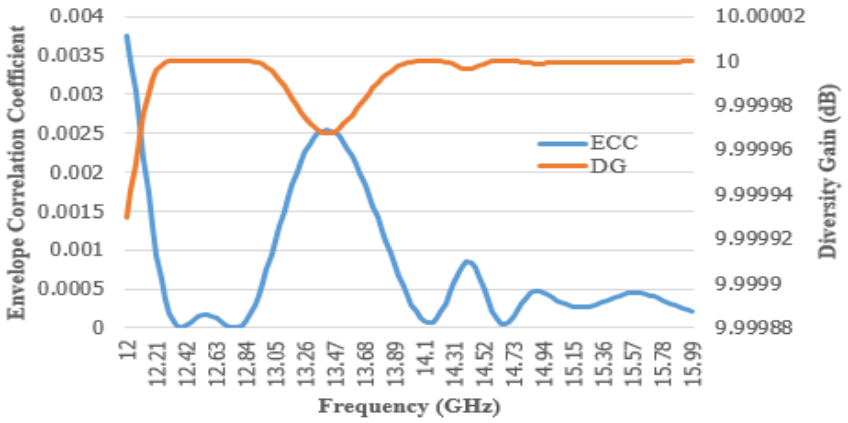

Fig. 9. Simulated DG of the proposed Antenna

e. Radiation Patterns

Figure 10 depicts the simulated radiation patterns of the proposed antenna at 12.3 GHz, 14.2 GHz, and 15 GHz for φ = 0° and φ = 90° planes. It can be seen that the antenna has stable radiation characteristics at the three operating frequencies. The direction of the main lobe is unchanged, showing stable radiation characteristics. The radiation pattern changes slightly with the change in frequency, which is expected for a multiband antenna. In general, the proposed antenna has stable and satisfactory radiation characteristics in the operating bands.

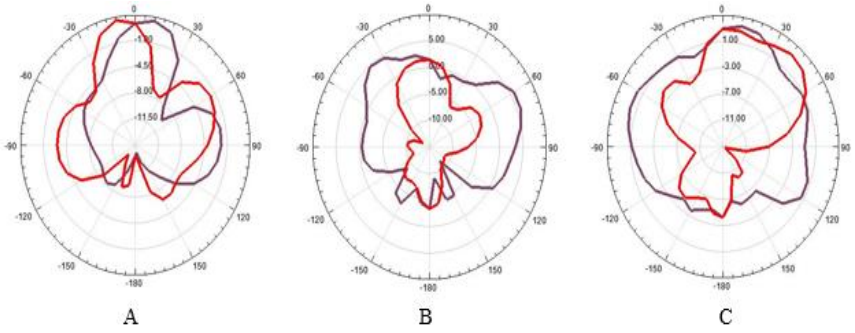

Fig. 10. Simulated radiation patterns of the proposed antenna at (A) 12.3 GHz, (B) 14.2 GHz, and (C) 15 GHz for φ = 0° (red) and φ = 90° (purple) planes.

IV. Fabrication and Measurement

In order to confirm the simulated performance of the proposed tri-band MIMO star microstrip patch antenna, a prototype of the final version (Antenna 3) was built and experimentally tested. Production was carried out on an FR4 substrate with dielectric constant εr = 4.4, thickness h = 1.6 mm, and overall dimensions of 41.5 x 30 mm^2. To achieve the star patch shape, standard PCB etching methods were used, while the ground plane was kept flat to maintain the optimal performance observed in the simulations. To feed the ports, two 50 Ω SMA connectors were soldered, both placed on the same side according to the final configuration. Figure 9 shows the fabricated

prototype, including the top view of the radiating patch and the bottom view of the ground plane.

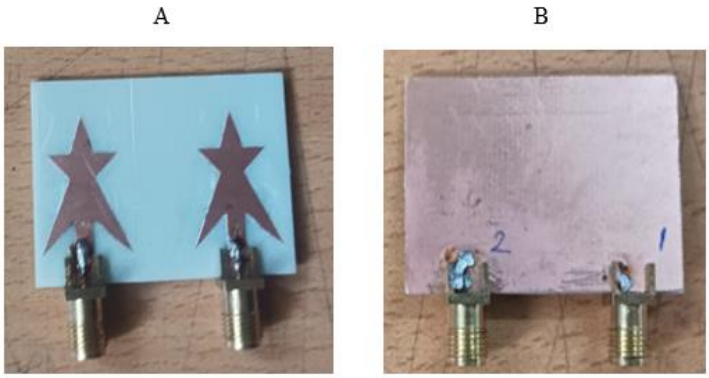

Fig. 11. Fabricated prototype (A) top view and (B) ground plane

The fabricated prototype was experimentally tested using a Vector Network Analyzer (VNA) across the 12–16 GHz frequency range. Both antenna ports were connected through 50-Ω SMA connectors, and a full two-port calibration was carried out before measurement. The evaluation included the reflection coefficients (S11 and S22), the transmission coefficient (S21), the Voltage Standing Wave Ratio (VSWR), and the input impedance at both ports. The measured results confirmed the triband behaviour, with resonances appearing close to the simulated frequencies. A slight frequency shift was observed in the measured curves compared to the simulated ones, which can be attributed to fabrication tolerances, soldering effects of SMA connectors, and variations in the effective permittivity of the FR4 substrate.

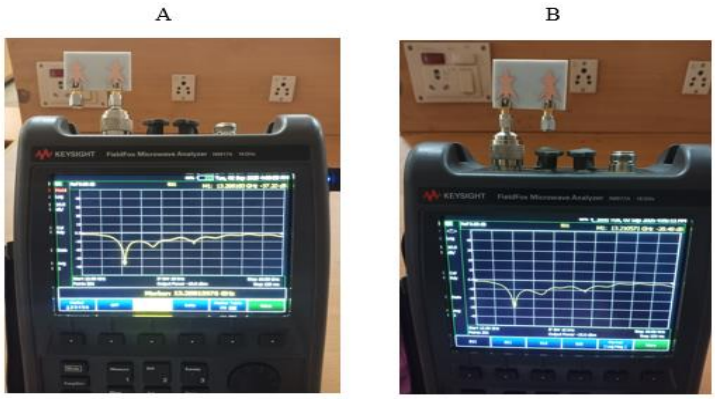

Fig. 12. Measurement of the prototype using VNA (A) Port 1 and (B) Port 2

The reflection coefficients (S11 and S22) exhibited values comparable to those obtained in simulation, validating the proper impedance matching of both ports. Furthermore, the measured VSWR remained consistently below 2 across the three operating bands, indicating that the antenna maintains good impedance matching throughout its operating range. The **measured input impedances** at the resonant frequencies were found to be **51.9 - j2.8 Ω** for port 1 and **51.2 - j0.5 Ω** for port 2. These values are remarkably close to the theoretical 50-Ω reference line used for system

matching. The small reactive components (-j2.8 and -j0.5 Ω) indicate only a minor deviation from the ideal purely resistive impedance, which confirms that the antenna is well matched across the operating bands.

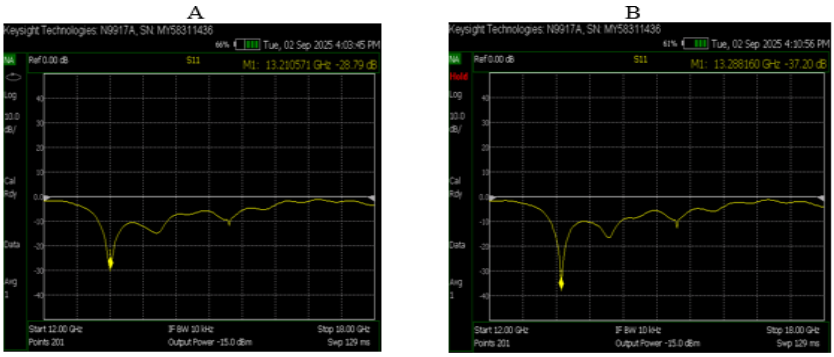

Fig. 13. The reflection coefficient of the fabricated antenna (A) S11 and (B) S22

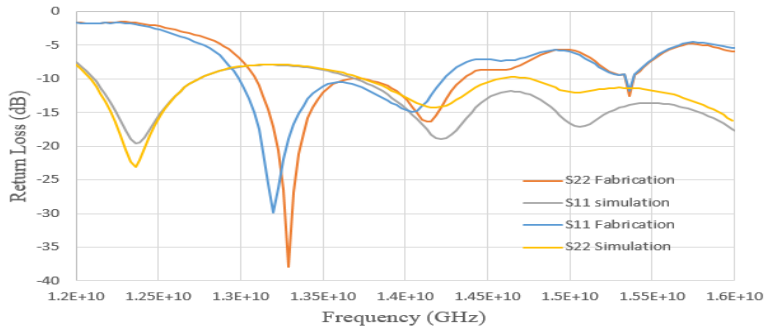

Fig. 14. Comparison of the reflection coefficient of the simulated and fabricated antenna

The simulated and measured realized gain of the fabricated antenna is presented in Fig. 15. The measured results confirm the trend of the simulated ones, with a slight decrease in gain. This variance is due to the fabrication tolerances, the connector losses, and the FR-4 substrate dielectric losses in Ku-band. The observed degradation in measured gain further confirms the impact of substrate losses.

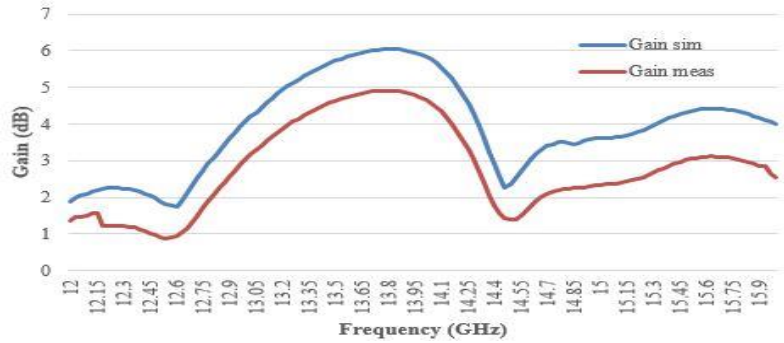

Fig. 15. Comparison of the gain between the simulated and measured values of the proposed antenna

Nevertheless, a good agreement between simulation and measurement is obtained, which confirms the proposed antenna design.

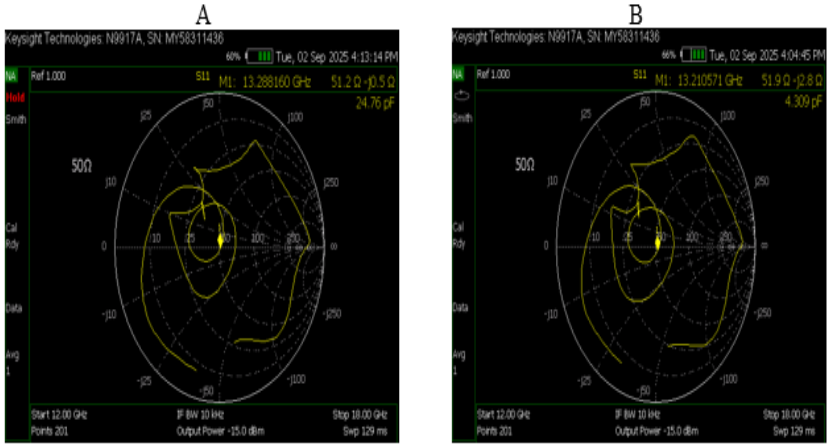

Fig. 16. Smith diagram of the input impedances (A) Port 1 and (B) Port 2

Table 2: Comparison with Other Works

Reference (Year)	Antenna type-configuration	Dimensions (mm^3)	Substrate	Target bands	Max Gain (dB)	Efficiency (%)	Isolation (dB)
[XII]	Tri-band with metamaterial loading	36 x 36 x 1.6	Rogers RT-5880	Ku band	5.0	70	-18
[VIII]	Tri-band MIMO, wide coverage	60 x 55 x 1.2	Rogers RT-5880	Ku band	6.2	65	-15
[XIII]	4-port shared radiator	25 x 22 x 0.5	Rogers RT-5880	X / Ku bands	5.8	72	-15
[VI]	Tri-band with DGS / fractal	12 x 14 x 0.8	Rogers RT-5880	C / X / Ku bands	7.8	70	-17

[IX]	3×2 MIMO array, 3D configuration	70 x 70 x 1.6	Rogers RT-5880	Ku band	7.3	75	-25
[XVII]	Compact quad-port MIMO	37.8 x 37.8 x 0.5	FR-4, εr = 4.4	Ku band	6.0	68	-20
[XIV]	4-port + FSS decoupler	25.7 x 25.7 x 0.8	Rogers RO4003 C	X / Ku bands	6.5	72	-23
This work - Antenna **3**	Triband star-shaped MIMO (2 ports)	41.5 x 30 x 1.6	FR-4, εr = 4.4	Ku-band	6.18	68	-32.5

The comparison with recent works highlights the distinctive advantages of the proposed design. In terms of compactness, the antenna occupies a moderate footprint of 41.5 x 30 mm², which is competitive compared to larger tri-band or multi-port MIMO designs that often exceed 60 mm in one dimension. By contrast, the present work demonstrates effective Ku-band triband operation on a low-cost FR-4 substrate, which is more suitable for mass production and practical integration. Overall, the results confirm that the proposed star-shaped MIMO triband antenna achieves a unique balance between size, cost-effectiveness, gain, and outstanding isolation, making it a highly competitive solution for Ku-band applications such as satellite communications and emerging 5G systems.

V. Conclusion

A star-shaped triband MIMO microstrip antenna for Ku-band applications has been designed, fabricated, and tested. The antenna operates at 12.3, 14.2, and 15.0 GHz, achieving a maximum gain of 6.18 dB, radiation efficiency of about 68%, and an excellent measured isolation of −32 dB. Compared with recent designs, the proposed antenna offers a competitive compromise between compact size, cost-effective FR-4 substrate, multiband operation, and superior isolation, making it a strong candidate for satellite and 5G Ku-band systems.

Conflict of Interest

There was no relevant conflict of interest regarding this article.

References

I. Alharbi, A. G., A. S. Alnahwi, and A. Sebak. "Compact Triband MIMO Antenna with High Isolation for 5G and Ku-Band Applications." IET Microwaves, Antennas & Propagation, vol. 15, 2021. 10.1007/s00339-023-07249-x.

II. Alibakhshikenari, M., et al. "Millimeter-Wave MIMO Array with Low Interactions Between Its Elements for 5G Communications." International Journal of Infrared and Millimeter Waves, 2025. 10.1007/s10762-025-01062-8.

III. Amraoui, Y., et al. "High Isolation Integrated Four-Port MIMO Antenna for Terahertz Applications." Results in Engineering, 2025. 10.1016/j.rineng.2025.105253

IV. Azari-Nasab, T., et al. "Triple-Band Operation Achievement via Multi-Input Multi-Output Antenna for Wireless Communication System Applications." International Journal of Microwave and Wireless Technologies, vol. 12, 2020, pp. 259–266. 10.1017/S1759078719001302.

V. Cheng, Y., et al. "A Compact 4-Element MIMO Antenna for Terminal Devices." Microwave and Optical Technology Letters, vol. 62, 2020, pp. 2930–2937. 10.1002/mop.32396.

VI. Din, I. U., et al. "A Compact Four-Element Multiple-Input Multiple-Output Array with an Integrated Frequency Selective Surface for Millimeter-Wave Applications." Telecom, vol. 6, 2025, p. 73. 10.3390/telecom6040073.

VII. El Hadri, D., et al. "High Isolation and Ideal Correlation Using Spatial Diversity in a Compact MIMO Antenna for Fifth-Generation Applications." International Journal of Antennas and Propagation, 2020, pp. 1–9. 10.1155/2020/2740920.

VIII. Ghawbar, F., et al. "Highly Self-Isolated 12×12 MIMO Antenna Elements for 5G Mobile Applications." Electronics, vol. 14, no. 7, 2025, p. 1424. 10.3390/electronics14071424

IX. Kamal, M. M., et al. "A Novel Hook-Shaped Antenna Operating at 28 GHz for Future 5G mmWave Applications." Electronics, vol. 10, 2021, p. 673. 10.3390/electronics10060673.

X. Kaneko, T. "Millimeter-Wave Digital Beam-Forming Massive-MIMO and Distributed-MIMO Technologies and Their Verifications Toward 5G-Beyond Further Capacity Enhancement." 2021 51st European Microwave Conference (EuMC), 2022, p. 605. 10.23919/EuMC50147.2022.9784320.

XI. Khan, I., et al. "Enhanced Quad-Port MIMO Antenna Isolation with Metamaterial Superstrate." IEEE Antennas and Wireless Propagation Letters, vol. 23, 2024, pp. 439–443. 10.1109/LAWP.2023.3328002.

XII. Khaddaj Mallat, N., et al. "Millimeter-Wave in the Face of 5G Communication: Potential Applications." IETE Journal of Research, 2020, pp. 1–9. 10.1080/03772063.2020.1714489.

XIII. Kumar, K., et al. "Self-Quadruplexing Circularly Polarized SIW Cavity-Backed Slot Antennas." IEEE Transactions on Antennas and Propagation, vol. 68, 2020, pp. 6419–6423. 10.1109/TAP.2020.2970101.

XIV. Kumar, Rajeev, G. S. Saini, and D. Singh. "Compact Tri-Band Patch Antenna for Ku-Band Applications." Progress in Electromagnetics Research C, vol. 103, 2020, pp. 45–58. 10.2528/PIERC20013101.

XV. Kothavari, P. K., et al. "A Novel Four-Port MIMO Antenna with Integrated Parasitic Elements for 5G NR Applications." Results in Engineering, 2025. 10.1016/j.rineng.2025.108235

XVI. Kumar, A., et al. "Development of Semi-Circular Corner Cut MIMO Antenna for 5G and 6G Applications." Results in Engineering, 2025. 10.1016/j.rineng.2024.103805

XVII. Lei, L., et al. "A Compact Wideband MIMO Antenna with Enhanced Isolation for X-Band Applications." 2025 IEEE International Symposium on Antennas and Propagation and North American Radio Science Meeting (AP-S/CNC-USNC-URSI), 2025, pp. 1584–1587. 10.1109/AP-S/CNC-USNC-URSI55537.2025.11266838.

XVIII. Li, H., et al. "A Wideband Dual-Polarized Endfire Antenna Array with Overlapped Apertures and Small Clearance for 5G Millimeter-Wave Applications." IEEE Transactions on Antennas and Propagation, vol. 69, 2023, pp. 815–824. 10.1109/TAP.2020.3016512.

XIX. Munir, M. E., et al. "A Four Element mm-Wave MIMO Antenna System with Wide-Band and High Isolation Characteristics for 5G Applications." Micromachines, vol. 14, 2023, p. 776. 10.3390/mi14040776.

XX. Rahman, M. A., et al. "Metamaterial-Based Tri-Band Compact MIMO Antenna System for 5G IoT Applications with Machine Learning Performance Verification." Scientific Reports, vol. 15, 2025, p. 22866. 10.1038/s41598-025-06391-1.

XXI. Ravi Sankar, C. V., et al. "A Star-Shaped Compact Tri-Band Antenna Design for C, X and Ku-Band Applications." Proceedings of ICEEICT, 2024, pp. 1–5. 10.1109/ICEEICT61591.2024.10718601.

XXII. Sehrai, D. A., et al. "A Novel High Gain Wideband MIMO Antenna for 5G Millimeter Wave Applications." Electronics, vol. 9, 2020, p. 1031. 10.3390/electronics9061031.

XXIII. Senthilkumar, S., et al. "A Compact Phased Array Antenna for 5G MIMO Applications." Wireless Personal Communications, vol. 128, 2023, pp. 2155–2174. 10.1007/s11277-022-10037-0.

XXIV. Sharma, V., R. K. Gangwar, and S. K. Koul. "Dual-Polarized MIMO Antenna with Defected Ground for Ku-Band Satellite Applications." IEEE Access*, vol*. 9, 2021, pp. 121340–121348. 10.1109/INSPECT63485.2024.10896085.

XXV. Suyama, S., et al. "Recent Studies on Massive MIMO Technologies for 5G Evolution and 6G." 2022 IEEE Radio and Wireless Symposium (RWS)*,* 2022, pp. 90–93. 10.1109/RWS53089.2022.9719949.

XXVI. Tao, J., and Q. Feng. "Compact Ultrawideband MIMO Antenna with Half-Slot Structure*."* IEEE Antennas and Wireless Propagation Letters*,* vol. 16, 2017, pp. 792–795. 10.1109/LAWP.2016.2604344.

XXVII. Zhang, Y., X. Li, and H. Wang. "High-Gain Dual-Band Antenna Array for Ku-Band Satellite Communication." IEEE Antennas and Wireless Propagation Letters*,* vol. 23, 2024, pp. 471–475. 10.1109/ICMMT61774.2024.10672214.